Nonequilibrium dual-boson approach

Feng Chen [1,*] Mikhail I. Katsnelson [2,†] and Michael Galperin [3,‡]
[1]*Department of Physics, University of California San Diego, La Jolla, California 92093, USA*
[2]*Radboud University Nijmegen, Institute for Molecules and Materials, 6525AJ Nijmegen, The Netherlands*
[3]*Department of Chemistry & Biochemistry, University of California San Diego, La Jolla, California 92093, USA*

(Received 17 December 2019; revised manuscript received 23 May 2020; accepted 11 June 2020; published 24 June 2020)

We develop a nonequilibrium auxiliary quantum master equation dual-boson method (aux-DB) and argue that it presents a convenient way to describe steady states of correlated impurity models (such as single-molecule optoelectronic devices) where electron and energy transport should be taken into account. The aux-DB is shown to provide high accuracy with relatively low numerical cost. Theoretical analysis is followed by illustrative simulations within generic junction models, where the scheme is benchmarked against numerically exact results.

DOI: 10.1103/PhysRevB.101.235439

I. INTRODUCTION

The fast development of nanofabrication techniques combined with advances in laser technology have led to tremendous progress in optical studies of nanoscale systems. Optical spectroscopy of single molecules in current-carrying junctions has become reality. Surface-enhanced [1–3] and tip-enhanced [4–6] Raman spectroscopies (SERS and TERS) as well as bias-induced electroluminescence [7–13] measurements yield information on the extent of heating of vibrational and electronic degrees of freedom in biased junctions, electron transport noise characteristics, molecular structure, dynamics, and chemistry. The combination of molecular electronics with nonlinear optical spectroscopy has resulted in the emergence of a new field of research coined optoelectronics [14,15].

The optical response of single-molecule junctions is only possible due to the strong enhancement of the signal by surface plasmons [16]. Large fields and confinement result in a strong interaction between molecular and plasmonic excitations. Note, also, the recent experiments on ultrastrong light-matter interaction in single-molecule nanocavities (at the moment, in the absence of electron current) [17,18]. At the nanoscale, classical electrodynamics becomes inadequate as it cannot describe quantum coherence and mixing between plasmon and molecular exciton, while strong interactions require one to go beyond perturbation theory.

The development of theoretical methods for the simulation of strongly correlated open nonequilibrium impurity systems is a prerequisite to model nanoscale molecular devices with potential applications from optical characterization and control to energy harvesting, spintronics, and quantum computation. With numerically exact techniques, such as continuous time quantum Monte Carlo [19–21] or renormalization group methods [22–25], being computationally costly and thus mostly focused on simple models, relatively numerically inexpensive and sufficiently accurate schemes for realistic simulations are in high demand.

One such universal impurity solver is the nonequilibrium dual-fermion (DF) approach originally introduced in Ref. [26]. Recently, the approach was modified [27] to reduce computational cost and improve the ability to simulate steady states of correlated impurity models. Note that the focus of the dual-fermion approach is electron transport. At the same time, simulations of optoelectronic devices require accounting for energy transfer also.

Here, we introduce the *auxiliary quantum master equation nonequilibrium dual-boson (aux-DB) method*, which is a universal nonequilibrium impurity solver that accounts for both charge and energy transport in strongly correlated open systems. Similar to the DF of Ref. [26] being the nonequilibrium version of the equilibrium DF method [28–31] (DF-inspired superperturbation theory), aux-DB has its origin in the equilibrium DB approach [32–39]. Below, after introducing the nonequilibrium DB in Sec. II, in Sec. III we present an auxiliary quantum master equation (QME) treatment within the method. Theoretical considerations are followed by illustrative numerical simulations within generic junction models in Sec. IV. Section V concludes.

II. NONEQUILIBRIUM DB THEORY

Here we present a short description of the aux-DB method. Detailed derivations are given in Appendix A. Similar to the DF method, in the nonequilibrium DB approach, one considers the reduced dynamics of an open quantum system with interactions confined to the molecular subspace. Contrary to the DF method, in addition to contacts (Fermi baths) the system is also coupled to Bose bath(s). The effect of the baths enters the effective action defined on the Keldysh contour [40] via corresponding self-energies Σ (for Fermi baths) and Π (for Bose baths),

$$S[\bar{d},d]=\bar{d}_1\left[G_0^{-1}-\Sigma^B\right]_{12}d_2-\bar{b}_1\,\Pi^B_{12}\,b_2+S^{\rm int}[\bar{d},d]. \quad (1)$$

*fec011@ucsd.edu
†M.Katsnelson@science.ru.nl
‡migalperin@ucsd.edu

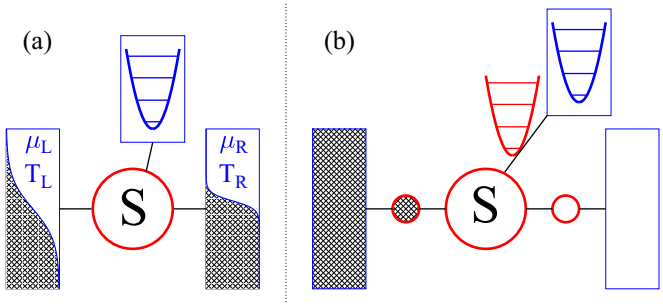

FIG. 1. Nonequilibrium junction model. Shown are (a) physical model and (b) reference system within aux-DB approach.

Here and below, summation of repeating indices is assumed. In (1), $\bar{d}_i \equiv \bar{d}_{m_i}(\tau_i)$ $[d_i \equiv d_{m_i}(\tau_i)]$ is the Grassmann variable corresponding to the creation [annihilation] operator $\hat{d}^\dagger_{m_i}(\tau_i)$ $[\hat{d}_{m_i}(\tau_i)]$, which represents both molecular (spin-) orbital m_i and contour variable τ_i, of an electron in orbital m_i in the Heisenberg picture [41]. $b_i = b_{m_1^i m_2^i}(\tau_i) \equiv \bar{d}_{m_1^i}(\tau_i) d_{m_2^i}(\tau_i)$ is the molecular excitation representing the optical transition within the molecule from orbital m_2^i to orbital m_1^i at contour variable τ_i. The sum over indices includes the summation over molecular orbitals (optical transitions) and contour integration: $\sum_i \ldots \equiv \sum_{m_i} \int_c d\tau_i \ldots$ $(\sum_{m_1^i, m_2^i} \int_c d\tau_i \ldots)$. G_0^{-1} is the inverse free Green's function (GF) [42],

$$\left[G_0^{-1}\right]_{12} \equiv \delta(\tau_1, \tau_2)\left[i\partial_{\tau_1}\delta_{m_1,m_2} - H^0_{m_1 m_2}(\tau_1)\right] - \Sigma^{\rm irr}_{12}, \quad (2)$$

and Σ^B and Π^B are, respectively, self-energies due to coupling to Fermi (contacts) and Bose (plasmon) baths,

$$\begin{aligned} \Sigma^B_{m_1 m_2}(\tau_1, \tau_2) &= V_{m_1 k} g_k(\tau_1, \tau_2) V_{k m_2}, \\ \Pi^B_{m_1 m_2, m_3 m_4}(\tau_1, \tau_2) &= V_{m_1 m_2, \alpha} d_\alpha(\tau_1, \tau_2) V_{\alpha, m_3 m_4}. \end{aligned} \quad (3)$$

In Eqs. (2) and (3), $H^0_{m_1 m_2}(\tau)$ is the noninteracting part of the molecular Hamiltonian, $\Sigma^{\rm irr}_{m_1 m_2}(\tau_1, \tau_2) \sim \delta(\tau_1, \tau_2)$ is the irregular self-energy, V_{mk} and $V_{m_1 m_2, \alpha}$ are matrix elements for the electron transfer from contact state k to molecular orbital m, and for optical electron transfer from orbital m_1 to m_2 with absorption of phonon in mode α, respectively. Here, $g_k(\tau_1, \tau_2) \equiv -i\langle T_c\, \hat{c}_k(\tau_1)\, \hat{c}^\dagger_k(\tau_2)\rangle$ and $d_\alpha(\tau_1, \tau_2) \equiv -i\langle T_c\, \hat{a}_\alpha(\tau_1)\, \hat{a}^\dagger_\alpha(\tau_2)\rangle$ are GFs of the free electron in state k of the contacts and free phonon in mode α. All intramolecular interactions are within the (unspecified) contribution to the action $S^{\rm int}[\bar{d}, d]$.

As in equilibrium DB [33], one introduces an exactly solvable *reference system* (see below). Similarly to aux-DF [27], the true baths are approximated by a finite number of auxiliary discrete modes subject to Lindbladian evolution [see Fig. 1(b)]. Thus, action of the reference system $\tilde{S}[\bar{d}, d]$ is known and has the same general form (1) with true self-energies Σ^B and Π^B substituted by their approximate representations $\tilde{\Sigma}^B$ and $\tilde{\Pi}^B$. The desired action S can then be written as

$$S[\bar{d}, d] = \tilde{S}[\bar{d}, d] + \bar{d}_1\, \delta\Sigma^B_{12}\, d_2 + \bar{b}_1\, \delta\Pi^B_{12}\, b_2, \quad (4)$$

where $\delta\Sigma^B \equiv \tilde{\Sigma}^B - \Sigma^B$ and $\delta\Pi^B \equiv \tilde{\Pi}^B - \Pi^B$.

Because direct application of the standard diagrammatic expansion around the interacting reference system is not possible (the Wick's theorem does not apply [43]), two artificial particles, *dual fermion* (f) and *dual boson* (η), are introduced which are used to unravel the last two terms in (4) via the Hubbard-Stratonovich transformation [44]. Integrating out molecular fermions (d and $\bar{d}$) and comparing the fourth-order cumulant expansion of the resulting expression with the general form of action for dual particles,

$$\begin{aligned} S^D[f^*, f] = \bar{f}_1 \left[\left(G_0^{DF}\right)^{-1} - \Sigma^{DF}\right]_{12} f_2 \\ + \bar{\eta}_1 \left[\left(D_0^{DB}\right)^{-1} - \Pi^{DB}\right]_{12} \eta_2, \end{aligned} \quad (5)$$

one gets

$$\begin{aligned} \left(G_0^{DF}\right)^{-1}_{12} &= -g^{-1}_{12} - g^{-1}_{13}\, [\delta\Sigma^B]^{-1}_{34}\, g^{-1}_{42}, \\ \left(D_0^{DB}\right)^{-1}_{12} &= -\chi^{-1}_{12} - \chi^{-1}_{13}\, [\delta\Pi^B]^{-1}_{34}\, \chi^{-1}_{42}, \\ \Sigma^{DF}_{12} &= \big\{\Gamma_{13;42} + i(\gamma_{514}\, \delta_{326} - \gamma_{512}\, \delta_{346} \\ &\quad + \gamma_{532}\, \delta_{146} - \gamma_{534}\, \delta_{126})\left[D_0^{DB}\right]_{65}\big\}\left[G_0^{DF}\right]_{43} \\ &\quad - \left(\langle \hat{b}^\dagger_5\rangle \chi^{-1}_{54} \gamma_{312} + \chi^{-1}_{35} \langle \hat{b}_5\rangle \delta_{124}\right)\left[D_0^{DB}\right]_{43}, \\ \Pi^{DB}_{12} &= -i\, \gamma_{145}\, \delta_{632}\left[G_0^{DF}\right]_{34}\left[G_0^{DF}\right]_{56}. \end{aligned} \quad (6)$$

Here, g_{12} and χ_{12} are single-particle GFs of fermion and molecular excitation of the reference system, and γ_{123}, δ_{123}, and $\Gamma_{13;24}$ are vertices [45] see Eq. (A12) and Fig. 5 in Appendix A.

With dual-particle GFs,

$$\begin{aligned} (G^{DF}) &= \left[\left(G_0^{DF}\right)^{-1} - \Sigma^{DF}\right]^{-1}, \\ (D^{DB}) &= \left[\left(D_0^{DB}\right)^{-1} - \Pi^{DB}\right]^{-1}, \end{aligned} \quad (7)$$

known, the single-particle (G) and two-particle (D) GFs of the molecule are obtained from

$$\begin{aligned} G &= (\delta\Sigma^B)^{-1} + [g\, \delta\Sigma^B]^{-1}\, G^{DF}\, [\delta\Sigma^B\, g]^{-1}, \\ D &= (\delta\Pi^B)^{-1} + [\chi\, \delta\Pi^B]^{-1}\, D^{DF}\, [\delta\Pi^B\, \chi]^{-1}. \end{aligned} \quad (8)$$

Note that the two-particle GF is a correlation function of the molecular optical excitation operators. G yields information on orbital populations, spectral functions, and electron current in the junction, while D is used in the calculation of boson (phonon) flux.

III. REFERENCE SYSTEM

Construction of a reference system to a large extent relies on accurate reproduction of the physical system's hybridization functions Σ^B and Π^B. The accurate choice of the reference system parameters was recently discussed in Refs. [46,47] for Bose baths and in Refs. [48–51] for Fermi baths. Here we combine both considerations by introducing, as the reference system, a physical system complemented with a finite number of auxiliary unitary modes (A) subject to Lindbladian evolution. This includes a finite number of sites representing Fermi baths and modes representing a Bose bath [see Fig. 1(b) and Appendix B]. The dynamics of the extended SA system (molecule plus finite number of sites and modes) is driven by Markov Lindblad-type evolution,

$$\frac{d\rho^{SA}(t)}{dt} = -i\mathcal{L}\rho^{SA}(t). \quad (9)$$

Here, $\rho^{SA}(t)$ is the extended system density operator and $\mathcal{L}$ is the Liouvillian. Note that Refs. [46] and [51] prove that, in principle, the Markov dynamics of the extended system can exactly reproduce non-Markov unitary dynamics of the physical system S as long as the free correlation function of the auxiliary modes accurately reproduces the correlation function of the full baths. However, in realistic calculations, this representation is approximate due to a restriction on number of auxiliary sites and modes which can be taken in consideration. Thus, the aux-DB accounting for the difference between true and reference system hybridization functions, given by Eq. (6), is very useful to correct the approximate mapping.

The aux-DB approach, given by Eqs. (5)–(8), requires single- and two-particle GFs g and χ and vertices Γ, γ, and δ of the reference system as an input. Those are obtained by solving the QME (9) and employing the quantum regression relation (see Appendix C for details).

Below we focus on the steady state and consider a reference system of size small enough that exact diagonalization can be employed. For larger systems, more advanced methods (e.g., matrix product states [49]) may be used. We note that while matrix product states (MPS) only work for one-dimensional (1D) problems, this does not impose limitation on the dimensionality of the original (physical) problem because any number and geometry of couplings in the physical problem can be mapped onto an effectively 1D formulation in the auxiliary reference system with only two (for Fermi) or one (for Bose) baths.

IV. NUMERICAL RESULTS AND DISCUSSION

Here we illustrate the aux-DB method with numerical simulations within generic junction models: the resonant level model (RLM) and Anderson impurity model (AIM) coupled to Fermi and Bose baths.

A. Model

We apply the aux-DB method to generic models with a junction constructed from a system S coupled to two Fermi (L and R) and one boson (P) bath [see Fig. 1(a)]. The Hamiltonian is

$$\hat{H} = \hat{H}_S + \sum_{B=L,R,P} (\hat{H}_B + \hat{V}_{SB}), \tag{10}$$

where

$$\begin{aligned} \hat{H}_{L(R)} &= \sum_{k\in L(R)} \varepsilon_k \hat{c}_k^\dagger \hat{c}_k, \\ \hat{H}_P &= \sum_{\alpha\in P} \omega_\alpha \hat{a}_\alpha^\dagger \hat{a}_\alpha \end{aligned} \tag{11}$$

are the Hamiltonians of the contact L (R) and phonon bath P. Also,

$$\begin{aligned} \hat{V}_{SL(R)} &= \sum_m \sum_{k\in L(R)} (V_{mk} \hat{d}_m^\dagger \hat{c}_k + \text{H.c.}), \\ \hat{V}_{SP} &= \sum_{m_1,m_2} \sum_{\alpha\in P} V_{m_1m_2}^\alpha (\hat{b}_{m_1m_2} + \hat{b}_{m_1m_2}^\dagger)(\hat{a}_\alpha + \hat{a}_\alpha^\dagger) \end{aligned} \tag{12}$$

describe the electron transfer between the system and contact L (R), and the coupling to phonon α in the thermal bath P, respectively. Here, $\hat{d}_m^\dagger$ ($\hat{d}_m$) and $\hat{c}_k^\dagger$ ($\hat{c}_k$) creates (annihilates) the electron in orbital m on the system and in state k of the contacts, respectively, $\hat{a}_\alpha^\dagger$ ($\hat{a}_\alpha$) creates (annihilates) the phonon in mode α, and $\hat{b}_{m_1m_2} = \hat{d}_{m_1}^\dagger \hat{d}_{m_2}$.

For the system Hamiltonian, we consider the resonant level model (RLM),

$$\hat{H}_S = \varepsilon_0 \hat{n}, \tag{13}$$

and Anderson impurity model (AIM),

$$\hat{H}_S = \sum_{m=1,2} \varepsilon_0 \hat{n}_m + U \hat{n}_1 \hat{n}_2. \tag{14}$$

Here, $\hat{n}_m = \hat{d}_m^\dagger \hat{d}_m$ and U is the Coulomb repulsion. In the AIM, two types of coupling to the thermal bath are considered: symmetric, $V_{m_1m_2}^\alpha = \delta_{m_1,m_2} V_{m_1}^\alpha$, and antisymmetric, $V_{m_1m_2}^\alpha = \delta_{m_1,m_2}(-1)^{m_1} V_{m_1}^\alpha$.

Using Eq. (8), we calculate single- and two-particle GFs and employ them to evaluate the spectral functions $A_m(E)$ electron current I_L [52] at the left interface and phonon energy flux J_P [15] out of the system

$$\begin{aligned} A_m(E) &= -\frac{1}{\pi} \text{Im}\, G_{mm}^r(E), \\ I_L &= -I_R = \int \frac{dE}{2\pi} \text{Tr}\big[\Sigma_L^<(E) G^>(E) - \Sigma_L^{B>}(E) G^<(E)\big], \\ J_P &= \int \frac{dE}{2\pi} E\, \text{Tr}[\Pi_P^<(E) D^>(E) - \Pi_P^>(E) D^<(E)] \end{aligned} \tag{15}$$

at the steady state. Here, $<$, $>$ and r are, respectively, lesser, greater, and retarded projections of the GFs, self-energies Σ and Π are defined in Eq. (3), and the trace is over molecular orbitals in expression for $I_{L(R)}$ and over intra-molecular transitions in expression for J_P.

The reference system for both models utilizes five auxiliary sites: four mediating coupling of the physical site to full and empty Fermi baths and one five-level system mediating coupling between the physical site and empty Bose bath [see Fig. 1(b) and Appendix B]. As mentioned earlier, bigger sizes of the auxiliary system require implementation of advanced methods (e.g., based on MPS) to solve the auxiliary QME. Here, we restrict our consideration to small sizes which can be evaluated by direct diagonalization of the Liouvillian. We note that while for such small size, representation of the physical hybridization function in the auxiliary system is of limited quality (see Fig. 6), the aux-DB superperturbation expansion in the difference of the two hybridization functions allows one to obtain high-quality results even for small reference system sizes.

B. Numerical results

We start from consideration of the RLM studied within the numerically exact quantum Monte Carlo (QMC) approach in Ref. [53]. Parameters (in arbitrary energy units E_0) are $k_BT = 0.2$ and $\varepsilon_0 = 3.2$. Following Ref. [53], Fermi baths are treated within the wide-band approximation (WBA) with a soft cutoff: $\Gamma_{L/R}(E) = \Gamma_{L/R}/[1 + e^{\nu(E-E_C)}][1 + e^{-\nu(E-E_C)}]$ with $\nu = 5$, $E_C = 20$ and $\Gamma_L = \Gamma_R = 0.5$; and the Bose bath

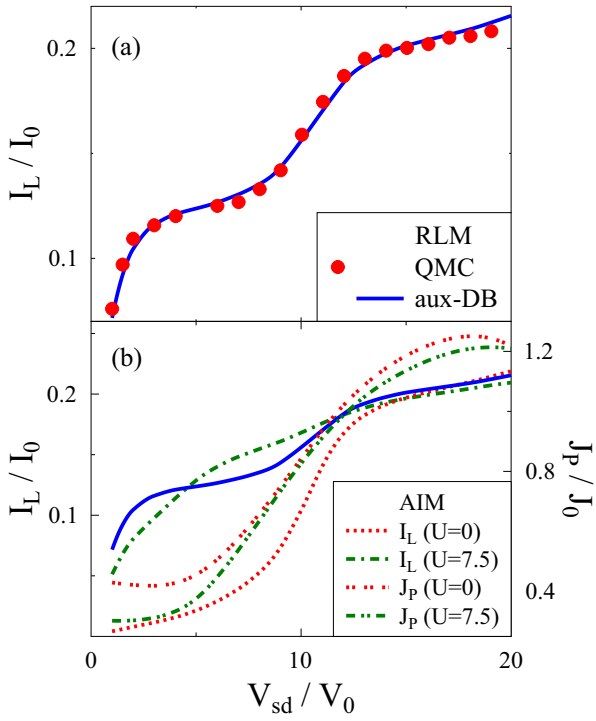

FIG. 2. Electron I_L and phonon J_P fluxes. Shown are results for the (a) RLM and (b) AIM. In (a), aux-DB results (solid blue line) are benchmarked vs the numerically exact QMC calculation of Ref. [53]. (b) Comparison of the aux-DB results for the AIM with $U = 0$ and $U = 7.5$. The solid blue line presents the RLM simulations within aux-DB and is the same in both panels.

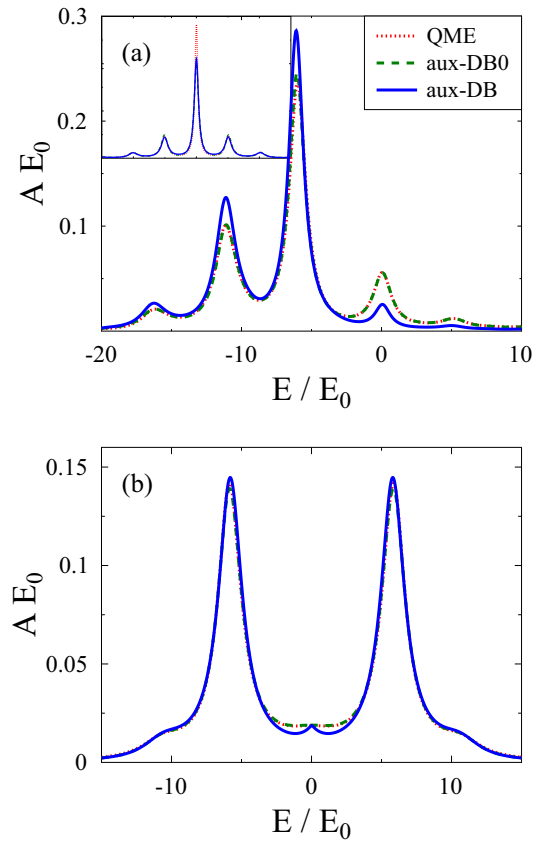

FIG. 3. Spectral function A for the AIM with (a) symmetric ($U = 0$, $V_{sd} = 6$) and (b) antisymmetric ($U = 5$, $V_{sd} = 0$) couplings to the thermal bath P. Shown are results of the auxiliary QME (dotted red line), zero-order (dashed green line), and first-order (solid blue line) aux-DB approaches. The inset in (a) shows the aux-DB results for the RLM.

is characterized by spectral density $J(\omega) = \gamma\omega/\{[(\omega/\omega_0)^2 - 1]^2 + [\gamma\omega_0\omega/(2M_0^2)]^2\}$ with $\gamma = 0.1$, $\omega_0 = 5$, and $M_0 = 4$. Bias was applied symmetrically: $\mu_L = -\mu_R = |e|V/2$. The results of the simulation are presented in terms of units of bias $V_0 = E_0/|e|$, flux $I_0 = E_0/\hbar$, and energy flux $J_0 = E_0^2/\hbar$. Figure 2(a) compares the aux-DB results (solid line) with the numerically exact QMC (circles) simulations of Ref. [53].

Aux-DB simulations of the AIM with symmetric coupling to the Bose bath for $U = 0$ (dotted line) and $U = 7.5$ (dashed line) Coulomb interaction are shown in Fig. 2(b). Note that even in the absence of Coulomb interaction, the results of simulations are significantly different from the results of the RLM (compare the dotted and solid lines). This is due to the effective electron-electron interaction induced by coupling to the common Bose bath and the effect can be understood within an effective negative-U model ($\tilde{\varepsilon}_0 = \varepsilon_0 - M_0^2/\omega_0$ and $\tilde{U} = U - 2M_0^2/\omega_0$), which predicts the doubly populated state $E_2 = 2\tilde{\varepsilon}_0 + \tilde{U} = -6.4$ to be the ground state of the $U = 0$ quantum dot with energy gap of 6 to its singly populated state $E_1 = \tilde{\varepsilon}_0 = 0$. This shows that the use of spinless models in studies of inelastic transport should be done with caution. For $U = 7.5$ (dash-dotted line), no current blockade is observed because the electron transition from the ground state is gapless. It is interesting to note that in a blockaded region, the energy (phonon) flux is higher than for resonant tunneling [compare the double-dotted and dash-double-dotted lines in Fig. 2(b)], which indicates the predominantly elastic character of resonant transport.

Figure 3 shows spectral functions simulated within the QME (dotted line), zero (dashed line), and first (solid line) aux-DB approaches for the cases of symmetric [Fig. 3(a)] and antisymmetric [Fig. 3(b)] couplings to the thermal bath. Figure 3(a) shows results for the AIM with $U = 0$, $M_0 = 4$ and symmetric coupling at $V_{sd} = 6$. The corresponding RLM results are given in the inset. While in the RLM aux-DB is already accurate in the zero order, the AIM $U = 0$ results are significantly renormalized when vertex corrections are taken into account. Figure 3(b) shows the results for the AIM with $k_BT = 0$, $U = 5$ and $\varepsilon_0 = -U/2$, $M_0 = 0.1$ and antisymmetric coupling at zero bias. One sees that in this case also, vertex corrections are important: they are necessary to reproduce the Kondo feature.

Figure 4(a) shows that Kondo is destroyed when increasing coupling strength M_0 to the thermal bath (compare the dotted and dashed lines). The effect is due to the bath-induced dephasing. Nonequilibrium simulation (solid line) shows the Kondo feature splitting. Finally, in Fig. 4(b), we show an increase of Coulomb peaks broadening with an increase of the coupling M_0. Here, parameters are $k_BT = 0$, $U = 5$, and $\varepsilon_0 = -U/2$, so that particle-hole symmetry is fulfilled. As previously noted, Fermi baths are considered within the WBA with $\nu = 10$ and $E_C = 20$. The Bose bath is taken to be ohmic:

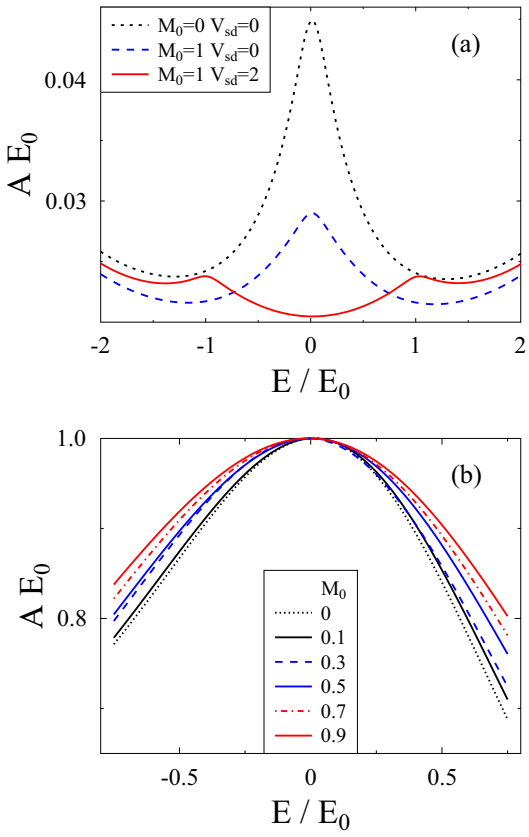

FIG. 4. Spectral function A of the AIM with antisymmetric coupling to thermal bath P. Shown are results for several molecule-thermal bath coupling strengths, with (a) destruction of the Kondo peak by dephasing induced by coupling to thermal bath and (b) broadening of the Coulomb peaks (for comparison, all Coulomb peaks are shifted to a common maximum set at $E = 0$).

$J(\omega) = M_0\,\omega\,e^{-\omega/\omega_C}$ with $\omega_C = 20$. To facilitate comparison, the peaks are shifted and scaled so that their maxima coincide and are equal to 1.

V. CONCLUSION

The nonequilibrium DF approach introduced originally in Ref. [26] and its optimization for steady-state simulations—the aux-DF approach [27]—are promising methods for modeling strongly correlated open systems. Contrary to the usual diagrammatic expansions, the methods can treat systems with no small parameter available. This is the situation often encountered in single-molecule optoelectronic devices, which are at the forefront of experimental and theoretical research due to interesting fundamental problems and applicational perspectives in energy nanomaterials, spintronics, and quantum computation. However, application of the aux-DF to simulations of optoelectronic devices is hindered by its inability to account for energy exchange between the molecule and plasmonic field. The latter is crucial in modeling of the devices.

Here we proposed a nonequilibrium method, *the aux-DB approach*, which accounts for both electron and energy fluxes between system and baths. The nonequilibrium aux-DB is a superperturbation theory inspired by the equilibrium DB method [32] proposed as a generalization of the extended dynamical mean-field theory (DMFT). Employing auxiliary QME and choosing an infinite reference system makes the approach advantageous in treating the steady states.

We utilized generic junction models of a molecule coupled to two Fermi leads and Bose phonon bath. The aux-DB was benchmarked vs the numerically exact QMC results of Ref. [53]. We showed that the scheme is both accurate and relatively numerically inexpensive. Further development of the method and its application to realistic systems is a goal for future research.

ACKNOWLEDGMENTS

M.G. acknowledges support by the National Science Foundation (Grant No. CHE-1565939). The work of M.I.K. is supported by the European Research Council via Synergy Grant No. 854843 - FASTCORR.

APPENDIX A: DERIVATION OF DUAL-BOSON EQUATIONS-OF-MOTION

Here we present the derivation of the expressions for the zero-order GFs, G_0^{DF} and D_0^{DB}, and self-energies, Σ^{DF} and Π^{DB}, for the dual-boson technique, given by Eq. (6) of the main text.

We consider a physical system which consists of the molecule (d) coupled to Fermi (c) and Bose (a) baths. Its partition function on the Keldysh contour is [40]

$$Z = \int_c D[\bar{d}, d, \bar{c}, c, \bar{a}, a]\, e^{iS[\bar{d},d,\bar{c},c,\bar{a},a]}, \tag{A1}$$

where

$$\begin{aligned} S[\bar{d}, d, \bar{c}, c, \bar{a}, a] = {} & \bar{d}_1 \left[G_0^{-1}\right]_{12} d_2 + S^{\rm int}[\bar{d}, d] + \bar{c}_1 \left[g_B^{-1}\right]_{12} c_2 \\ & + \bar{a}_1 \left[d_B^{-1}\right]_{12} a_2 + \bar{d}_1 V_{12} c_2 + \bar{c}_2 V_{21} d_1 \\ & + \bar{b}_1 V_{12} a_2 + \bar{a}_2 V_{21} b_1 \end{aligned} \tag{A2}$$

is the action of an interacting system (molecule) coupled to noninteracting contacts (Fermi bath) and plasmon (Bose bath). Here, G_0^{-1} is defined in Eq. (2) of the main text and g_B^{-1} and d_B^{-1} are the inverse GFs for free electrons in the contacts and free photons in the Bose bath,

$$\begin{aligned} \left[g_B^{-1}\right]_{12} &= \delta(\tau_1, \tau_2)\left[i\partial_{\tau_1} - \varepsilon_k\right], \\ \left[d_B^{-1}\right]_{12} &= \delta(\tau_1, \tau_2)\left[i\partial_{\tau_1} - \omega_\alpha\right]. \end{aligned} \tag{A3}$$

After integrating out the baths degrees of freedom [41], one gets the effective action presented in Eq. (1) of the main text.

Next, we introduce *an exactly solvable reference system*, which is identical to the original one in all intrasystem interactions, but differs from it by its hybridization function. The effective action of the original system will be related to that of the reference system via Eq. (4) of the main text. Because direct application of the perturbation theory to Eq. (4) is not possible, we apply two Hubbard-Stratonovich transformations to introduce new particles, *dual fermion* (f) and *dual boson* (η), which disentangle the last two terms in Eq. (4). Following

Ref. [33], we get

$$e^{\bar{d}_1 N_{12} d_2} = Z_f \int_c D[\bar{f}, f]\, e^{-\bar{f}_1 \alpha^f_{12} [N^{-1}]_{23} \alpha^f_{34} f_4 + \bar{f}_1 \alpha^f_{12} d_2 + \bar{d}_1 \alpha^f_{12} f_2},$$
$$e^{\bar{b}_1 M_{12} b_2} = Z_b \int_c D[\bar{\eta}, \eta]\, e^{-\bar{\eta}_1 \alpha^b_{12} [M^{-1}]_{23} \alpha^b_{34} \eta_4 + \bar{\eta}_1 \alpha^b_{12} b_2 + \bar{b}_1 \alpha^b_{12} \eta_2}, \tag{A4}$$

with

$$\alpha^f = i\, g^{-1}, \quad N = i\, \delta \Sigma^B, \quad Z_f = (\det [\alpha^f\, N^{-1}\, \alpha^f])^{-1},$$
$$\alpha^b = i\, \chi^{-1}, \quad M = i\, \delta \Pi^B, \quad Z_b = \det [\alpha^b\, M^{-1}\, \alpha^b]. \tag{A5}$$

Applying the transformation to the partition function (A1) with the action given by Eq. (4) of the main text yields

$$Z = Z_f\, Z_b \int_c D[\bar{d}, d, \bar{f}, f, \bar{\eta}, \eta] e^{iS[\bar{d}, d, \bar{f}, f, \bar{\eta}, \eta]}, \tag{A6}$$

where

$$\begin{aligned} &S[\bar{d}, d, \bar{f}, f, \bar{\eta}, \eta] \\ &\quad = \tilde{S}[d^*, d] - \bar{f}_1\, g^{-1}_{12}\, [\delta \Sigma^B]^{-1}_{23}\, g^{-1}_{34}\, f_4 + \bar{f}_1\, g^{-1}_{12}\, d_2 + \bar{d}_1\, g^{-1}_{12} f_2 \\ &\qquad - \bar{\eta}_1 \chi^{-1}_{12}\, [\delta \Pi^B]^{-1}_{23}\, \chi^{-1}_{34}\, \eta_4 + \bar{\eta}_1\, \chi^{-1}_{12}\, b_2 + \bar{b}_1\, \chi^{-1}_{12}\, \eta_2. \end{aligned} \tag{A7}$$

Thus, auxiliary quasiparticles—dual fermion (f) and dual boson (η)—were introduced.

Integrating out of the real quasiparticle, $\bar{d}$ and d, in (A6) leads to

$$Z = Z_f\, Z_b\, \tilde{Z} \int_c D[\bar{f}, f, \bar{\eta}, \eta] e^{iS[\bar{f}, f \bar{\eta}, \eta]}, \tag{A8}$$

with

$$\begin{aligned} S[\bar{f}, f \bar{\eta}, \eta] = \bar{f}_1 \left[G^{DF}_0\right]^{-1}_{12} f_2 + \bar{\eta}_1 \left[D^{DB}_0\right]^{-1}_{12} \eta_2 \\ + V[\bar{f}, f, \bar{\eta}, \eta]. \end{aligned} \tag{A9}$$

Here, $[G^{DF}_0]^{-1}_{12}$ and $[D^{DB}_0]^{-1}_{12}$ are defined in Eq. (6) of the main text, $\tilde{Z}$ is the partition function of the reference system, and $V[\bar{f}, f, \bar{\eta}, \eta]$ is the unknown interaction between dual particles.

To get the interaction $V[\bar{f}, f, \bar{\eta}, \eta]$, we expand (A6) in the $f - d$ and $\eta - b$ interactions and integrate out real quasiparticles, $\bar{d}$ and d. Taking g and χ to be single-electron and single-molecular excitation GFs of the reference system,

$$g_{12} = \frac{-i}{\tilde{Z}} \int_c D[\bar{d}, d]\, d_1 \bar{d}_2\, e^{i\tilde{S}[\bar{d}, d]} \equiv -i \langle T_c\, \hat{d}_1\, \hat{d}^\dagger_2 \rangle_{\rm ref},$$
$$\chi_{12} = \frac{-i}{\tilde{Z}} \int_c D[\bar{d}, d]\, \delta b_1\, \delta \bar{b}_2\, e^{i\tilde{S}[\bar{d}, d]} \equiv -i \langle T_c\, \hat{b}_1\, \hat{b}^\dagger_2 \rangle_{\rm ref}, \tag{A10}$$

and comparing the resulting expression to the expansion of (A8) yields the expression for $V[\bar{f}, f, \bar{\eta}, \eta]$. In particular, for expansion up to fourth order in $\bar{f}$, f and second order in $\bar{\eta}$, η,

$$\begin{aligned} V[\bar{f}, f, \bar{\eta}, \eta] = \bar{\eta}_1\, \chi^{-1}_{12}\, \langle b_2 \rangle_{\rm ref} + \langle \bar{b}_1 \rangle_{\rm ref}\, \chi^{-1}_{12}\, \eta_2 \\ - \frac{i}{4} \bar{f}_1\, \bar{f}_3 \Gamma_{13;24} f_2 f_4 - \bar{\eta}_1\, \gamma_{123}\, \bar{f}_2\, f_3 \\ - \bar{f}_3\, f_2\, \delta_{321}\, \eta_1. \end{aligned} \tag{A11}$$

Here, γ_{123}, δ_{321}, and $\Gamma_{13;24}$ are vertices of the reference system,

$$\begin{aligned} \Gamma_{13;24} &= g^{-1}_{1'1}\, g^{-1}_{3'3}\, [-\langle T_c\, \hat{d}_{1'}\, \hat{d}^\dagger_{2'}\, \hat{d}_{3'}\, \hat{d}^\dagger_{4'} \rangle_{\rm ref} - g_{1'2'}\, g_{3'4'} \\ &\quad + g_{1'4'}\, g_{3'2'}]\, g^{-1}_{2'2}\, g^{-1}_{4'4}, \\ \gamma_{123} &= \chi^{-1}_{11'}\, g^{-1}_{22'}\, \langle T_c\, \delta \hat{b}_{1'}\, \hat{d}_{2'}\, \hat{d}^\dagger_{3'} \rangle_{\rm ref}\, g^{-1}_{3'3}, \\ \delta_{321} &= g^{-1}_{33'}\, \langle T_c\, \hat{d}_{3'}\, \hat{d}^\dagger_{2'}\, \delta \hat{b}^\dagger_{1'} \rangle_{\rm ref}\, \chi^{-1}_{1'1}\, g^{-1}_{2'2}. \end{aligned} \tag{A12}$$

Here, T_c is the contour ordering operator, subscript ref indicates the Markov Lindblad-type evolution of the reference system, and $\delta \hat{b} \equiv \hat{b} - \langle \hat{b} \rangle_{\rm ref}$. We note in passing that projections of the vertices γ_{123} and δ_{321} are related via

$$\left[\gamma^{s_1 s_2 s_3}_{123}\right]^* = -\delta^{\bar{s}_3 \bar{s}_2 \bar{s}_1}_{321}, \tag{A13}$$

where $s_{1,2,3} \in \{-, +\}$ indicate branches of the Keldysh contour and $\bar{s}$ is the branch opposite to s.

Finally, using (A8) with interaction given by (A11) in the expansion of GFs for the dual particles,

$$G_{12} \equiv -i \langle T_c\, f_1\, \bar{f}_2 \rangle,$$
$$D_{12} \equiv -i \langle T_c\, b_1\, \bar{b}_2 \rangle, \tag{A14}$$

up to second order and employing the Wick's theorem yields the dual-particle self-energies given in Eq. (6) of the main text. The corresponding diagrams are shown in Fig. 5.

APPENDIX B: FITTING HYBRIDIZATION FUNCTIONS WITH AUXILIARY MODES

Recently, exact proof of the possibility to map unitary evolution of a physical system onto Markov Lindblad-type evolution of an auxiliary system was established for systems interacting with Fermi [48–51] and Bose [46,47] baths. At the heart of the mapping is the fitting of hybridization functions of the physical system with the set of auxiliary modes in the auxiliary system. Here, we give details of the fitting procedure.

The explicit form for the Markov Lindblad-type QME (9) is

$$\frac{d \rho^{SA}(t)}{dt} = -i \mathcal{L} \rho^{SA}(t) \equiv -i [\hat{H}_{SA}, \rho^{SA}(t)] + \mathcal{D} \rho^{SA}(t), \tag{B1}$$

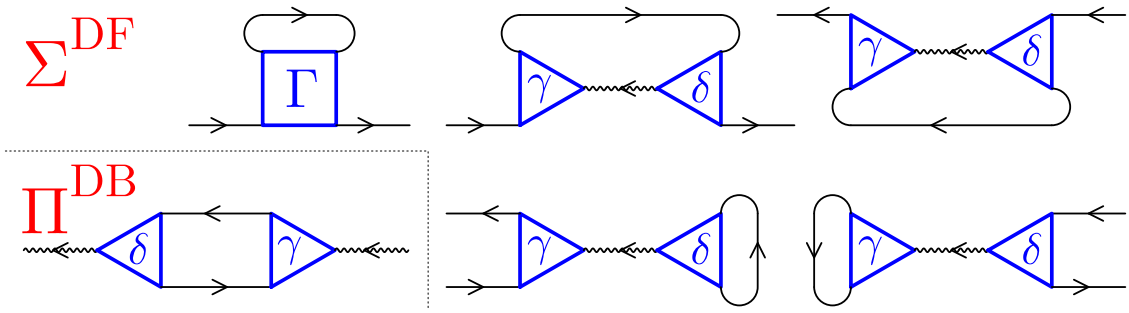

FIG. 5. Contributions to diagrams for dual fermion, Σ^{DF}, and dual boson, Π^{DB}, self-energies, given by Eq. (6). Directed solid and wavy lines (black) indicate dual-fermion and dual-boson GFs, G_0^{DF} and D_0^{DB}, respectively. The triangles and square (blue) indicate vertices δ, γ and Γ of the reference system.

with the Liouvillian taken as

$$\begin{aligned}\hat{H}_{SA} &= \hat{H}_S + \sum_{n_1,n_2} \epsilon_{m_1m_2}\hat{c}^\dagger_{n_1}\hat{c}_{n_2} + \sum_{m,n}(t_{mn}\hat{d}^\dagger_m\hat{c}_n + t^*_{mn}\hat{c}^\dagger_n\hat{d}_m)\\ &+ \sum_{\beta_1,\beta_2}\omega_{\beta_1\beta_2}\hat{e}^\dagger_{\beta_1}\hat{e}_{\beta_2} + \sum_{m_1,m_2,\beta} r^\beta_{m_1m_2}\big(\hat{b}^\dagger_{m_1m_2} + \hat{b}^\dagger_{m_1m_2}\big)\\ &\times (\hat{e}_\beta + \hat{e}^\dagger_\beta),\\ \mathcal{D}\rho &= \sum_{n_1,n_2}\Big[\Gamma^{(R)}_{n_1n_2}\Big(\hat{c}_{n_2}\,\hat{\rho}\,\hat{c}^\dagger_{n_1} - \frac{1}{2}\big\{\hat{\rho},\hat{c}^\dagger_{n_1}\hat{c}_{n_2}\big\}\Big)\\ &+ \Gamma^{(L)}_{n_1n_2}\Big(\hat{c}^\dagger_{n_1}\,\hat{\rho}\,\hat{c}_{n_2} - \frac{1}{2}\big\{\hat{\rho},\hat{c}_{n_2}\hat{c}^\dagger_{n_1}\big\}\Big)\Big]\\ &+ \sum_{\beta_1,\beta_2}\gamma^{(P)}_{\beta_1\beta_2}\Big(\hat{e}_{\beta_2}\,\hat{\rho}\,\hat{e}^\dagger_{\beta_1} - \frac{1}{2}\big\{\hat{e}^\dagger_{\beta_1}\hat{e}_{\beta_2},\hat{\rho}\big\}\Big).\end{aligned} \tag{B2}$$

Here, $\hat{c}^\dagger_n$ ($\hat{c}_n$) and $\hat{e}^\dagger_\beta$ ($\hat{e}_\beta$) create (annihilate) the excitation in auxiliary Fermi mode n and Bose mode β, respectively.

Following Refs. [49,51], we construct retarded $\tilde{\Sigma}^r$ and Keldysh $\tilde{\Sigma}^K$ projections of the Fermi hybridization function in the auxiliary system as

$$\begin{aligned}\tilde{\Sigma}^r_{m_1m_2}(E) &= \sum_{n_1,n_2} t_{m_1n_1}\,\tilde{G}^r_{n_1n_2}(E)\,t^*_{m_2n_2},\\ \tilde{\Sigma}^K_{m_1m_2}(E) &= \sum_{n_1,n_2} t_{m_1n_1}\,\tilde{G}^K_{n_1n_2}(E)\,t^*_{m_2n_2},\end{aligned} \tag{B3}$$

where

$$\begin{aligned}\tilde{\mathbf{G}}^r(E) &= \Big[E\,\mathbf{I} - \epsilon + \frac{i}{2}(\mathbf{\Gamma}^{(R)} + \mathbf{\Gamma}^{(L)})\Big]^{-1},\\ \tilde{\mathbf{G}}^K(E) &= i\,\tilde{\mathbf{G}}^r(E)\,(\mathbf{\Gamma}^{(L)} - \mathbf{\Gamma}^{(R)})\,\tilde{\mathbf{G}}^a(E)\end{aligned} \tag{B4}$$

are retarded $\tilde{\mathbf{G}}^r(E)$ and Keldysh $\tilde{\mathbf{G}}^K(E)$ projections of the Fermi auxiliary modes Green's functions, and where $\tilde{\mathbf{G}}^a(E) \equiv [\tilde{\mathbf{G}}^r(E)]^\dagger$ is its advanced projection. Hybridization functions (B3) should fit the corresponding hybridization functions,

$$\begin{aligned}\Sigma^r_{m_1m_2}(E) &= \sum_{k\in\{L,R\}} V_{m_1k}\,g^r_k(E)\,V_{km_2},\\ \Sigma^K_{m_1m_2}(E) &= \sum_{k\in\{L,R\}} V_{m_1k}\,g^K_k(E)\,V_{km_2},\end{aligned} \tag{B5}$$

of the physical system. Here,

$$\begin{aligned}g^r_k(E) &\equiv (E - \varepsilon_k + i\delta)^{-1},\\ g^K_k(E) &\equiv 2\pi i\,(2n_k - 1)\delta(E - \varepsilon_k)\end{aligned} \tag{B6}$$

are the retarded and Keldysh projections of the free electron in state k in contacts, n_k is the Fermi-Dirac thermal distribution, and $\delta = 0^+$

We construct the Bose hybridization function in the auxiliary system following Refs. [46,47]. For the physical system-bosonic bath coupling taken in the form

$$\sum_{m_1m_2}\sum_\alpha V^\alpha_{m_1m_2}\big(\hat{b}_{m_1m_2} + \hat{b}^\dagger_{m_1m_2}\big)(\hat{a}_\alpha + \hat{a}^\dagger_\alpha), \tag{B7}$$

the effect of the bosonic environment can be fully encoded by the correlation function,

$$\begin{aligned}&\Pi_{m_1m_2,m_3m_4}(t - t')\\ &\quad= \sum_\alpha V^\alpha_{m_1m_2}\,\langle(\hat{a}_\alpha + \hat{a}^\dagger_\alpha)(t)\,(\hat{a}_\alpha + \hat{a}^\dagger_\alpha)(t')\rangle\,V^\alpha_{m_3m_4}.\end{aligned} \tag{B8}$$

Similarly, coupling to auxiliary Bose modes in (B2) is fully described by the correlation function

$$\begin{aligned}&\tilde{\Pi}_{m_1m_2,m_3m_4}(t - t')\\ &\quad= \sum_{\beta_1,\beta_2} r^{\beta_1}_{m_1m_2}\big\langle\big(\hat{e}_{\beta_1} + \hat{e}^\dagger_{\beta_1}\big)(t)\,\big(\hat{e}_{\beta_2} + \hat{e}^\dagger_{\beta_2}\big)(t')\big\rangle\,r^{\beta_2}_{m_3m_4}\\ &\quad\equiv i\sum_{\beta_1,\beta_2} r^{\beta_1}_{m_1m_2}\big[\tilde{D}^>_{\beta_1\beta_2}(t - t') + \tilde{D}^<_{\beta_2\beta_1}(t' - t)\big].\end{aligned} \tag{B9}$$

Here, $\tilde{D}^>$ and $\tilde{D}^<$ are the greater and lesser projections of the Bose auxiliary mode Green's function,

$$\tilde{D}_{\beta_1\beta_2}(\tau_1,\tau_2) = -i\langle T_c\,\hat{e}_{\beta_1}(\tau_1)\,\hat{e}^\dagger_{\beta_2}(\tau_2)\rangle. \tag{B10}$$

The Fourier transform of the correlation function (B9) is

$$\tilde{\Pi}_{m_1m_2,m_3m_4}(E) = i\sum_{\beta_1,\beta_2} r^{\beta_1}_{m_1m_2}\big[\tilde{D}^>_{\beta_1\beta_2}(E) + \tilde{D}^<_{\beta_2\beta_1}(-E)\big]. \tag{B11}$$

According to Ref. [46], in the auxiliary system, one considers the Bose bath at zero temperature with eigenmodes spanning the energy range from $-\infty$ to $+\infty$. Thus, greater and lesser projections of the Green's function (B10) satisfy

$$\begin{aligned}\tilde{\mathbf{D}}^>(E) &= -i\,\tilde{\mathbf{D}}^r(E)\,\gamma^{(P)}\,\tilde{\mathbf{D}}^a(E),\\ \tilde{\mathbf{D}}^<(E) &= 0,\end{aligned} \tag{B12}$$

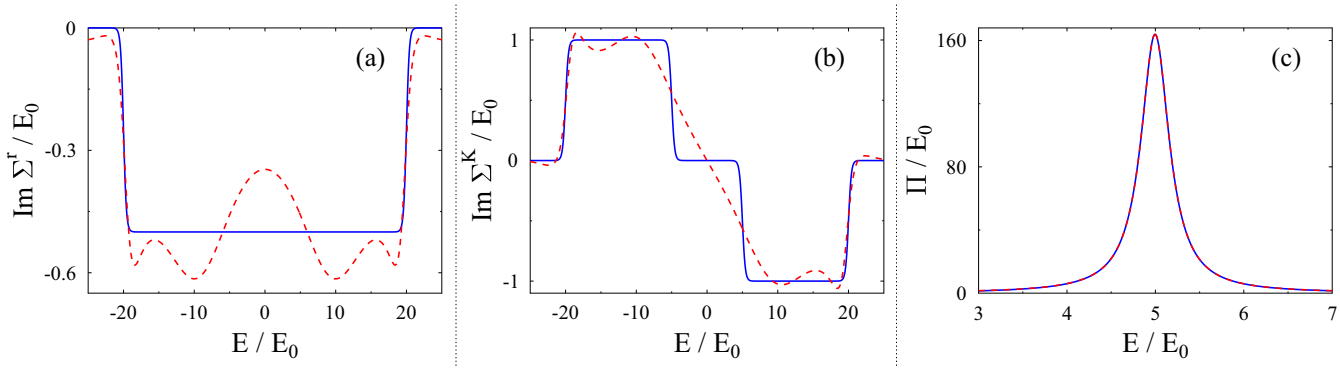

FIG. 6. Hybridization functions of the physical (solid blue line) and auxiliary (dashed red line) systems. Shown are the (a) retarded and (b) Keldysh projections of the self-energy due to coupling to contacts and (c) hybridization function due to coupling to the thermal bath. Fitting is done for parameters adopted in the first numerical example presented in the main text.

where

$$\tilde{\mathbf{D}}^r(E) = \left(E\,\boldsymbol{I} - \omega + \frac{i}{2}\gamma^{(P)}\right)^{-1}, \qquad \tilde{\mathbf{D}}^a(E) = [\tilde{\mathbf{D}}^r(E)]^\dagger \tag{B13}$$

are the retarded projection and advanced projections.

For the correlation function (B8) representing the physical system and for the case of a thermal Bose bath with inverse temperature β,

$$\Pi_{m_1m_2,m_3m_4}(E) = \left(1 + \coth\frac{\beta E}{2}\right)\big[J_{m_1m_2,m_3m_4}(E)\,\theta(E) - J_{m_3m_4,m_1m_2}(-E)\,\theta(-E)\big], \tag{B14}$$

where

$$J_{m_1m_2,m_3m_4}(E) \equiv \pi \sum_\alpha V^\alpha_{m_1m_2} V^\alpha_{m_3m_4}\,\delta(E-\omega_\alpha). \tag{B15}$$

Following Ref. [47], we stress that although the auxiliary Bose bath is taken at zero temperature, this does not restrict the temperature of the Bose bath in the physical system: the information about finite temperature will be provided by parameters of the auxiliary Bose modes.

Finally, note that parameters $\epsilon_{m_1m_2}$, t_{mn}, $\omega_{\beta_1\beta_2}$, $r^\beta_{m_1m_2}$, $\Gamma^{(L)}_{n_1n_2}$, $\Gamma^{(R)}_{n_1n_2}$, and $\gamma^{(P)}_{\beta_1\beta_2}$ of the Lindblad equations (B1) and (B2) are used to fit hybridization functions (B5) and (B14) of the physical system with corresponding hybridization functions (B3) and (B11) of the auxiliary model employing a cost function to quantify deviation [51]. Figure 6 shows the hybridization functions for the physical model (solid lines) and their fitting with auxiliary modes (dashed lines) as utilized in simulations of the RLM and AIM with symmetric coupling to the thermal bath presented in the main text. We used four Fermi and one Bose auxiliary modes to fit the corresponding hybridization functions.

APPENDIX C: GREEN'S FUNCTIONS AND VERTICES OF THE REFERENCE SYSTEM

To evaluate dual-particle self-energies, given by Eq. (6) of the main text, one has to calculate GFs g and χ, given by Eq. (A10), and vertices γ, δ, and Γ, given by Eq. (A12), of the reference system. These quantities are given by two- (g and χ), three- (γ, δ), and four-time (Γ) correlation functions defined on the Keldysh contour. To provide these, we utilize the quantum regression relation.

Because Markov Lindblad-type QME is used to solve the reference system, we can employ the quantum regression relation [54],

$$\langle T_c\,\hat{A}(\tau_1)\,\hat{B}(\tau_2)\ldots\hat{Z}(\tau_n)\rangle = \mathrm{Tr}[\mathcal{O}_n\,\mathcal{U}(t_n,t_{n-1})\ldots\mathcal{O}_2\,\mathcal{U}(t_2,t_1)\,\mathcal{O}_1\,\mathcal{U}(t_1,0)\,\rho^{SA}(0)], \tag{C1}$$

to evaluate the correlation functions. Here, $\rho^{SA}(0)$ is the steady-state density matrix of the extended system, $\mathcal{U}(t_i,t_{i-1})$ is the Liouville space evolution operator, and times t_i are ordered so that $t_n > t_{n-1} > \cdots > t_2 > t_1 > 0$. $\mathcal{O}_i$ is the Liouville space superoperator corresponding to one of the operators $\hat{A}\ldots\hat{Z}$ whose time is the i-th in the ordering. It acts from the left (right) for the operator on the forward (backward) branch of the contour. The steady-state density matrix is found as a right eigenvector $|R_0\gg$ corresponding to the Liouvillian eigenvalue $\lambda_0 = 0$. Using spectral decomposition of the Liouvillian, the evolution operator can be presented in its eigenbasis as

$$\mathcal{U}(t_i,t_{i-1}) = \sum_\gamma |R_\gamma\gg\, e^{-i\lambda_\gamma(t_i-t_{i-1})}\, \ll L_\gamma|. \tag{C2}$$

For evaluation of single- and two-particle GFs, besides the $\mathcal{L}$ of Eq. (9) of the main text, we will also need Liouvillians $\mathcal{L}^{(\pm1)}$ and $\mathcal{L}^{(\pm2)}$. These are evolution operator generators for Liouville space vectors $|S_1S_2\gg$ with different number N_S of electrons in states $|S_1\rangle$ and $|S_2\rangle$: $N_{S_1} - N_{S_2} = \pm1, \pm2$.

Using (C2) in (C1) yields expressions for the single-particle (g and χ) and two-particle GFs of the reference system. To do so, we have to consider several projections (contour orderings) and time orderings. In particular, evaluation of two-time correlation functions requires consideration of $2^1 = 2$ projections with $2! = 2$ time orderings for each projection. Three-time correlation functions will require consideration of $2^2 = 4$ projections with $3! = 6$ time orderings. Evaluation of the four-time correlation function requires consideration of $2^3 = 8$ projections with $4! = 24$ time orderings. Evaluating projections, one has to take care of the sign of the Fermi

operators permutations,

$$\langle T_c\, \hat{O}_1(\tau_1)\, \hat{O}_2(\tau_2) \dots \hat{O}_N(\tau_N)\rangle_{\rm ref} = (-1)^P \big\langle\!\big\langle I|\mathcal{O}_{\theta_1}\, \mathcal{U}\big(t_{\theta_1}, t_{\theta_2}\big)\, \mathcal{O}_{\theta_2}\, \mathcal{U}\big(t_{\theta_2}, t_{\theta_3}\big) \cdots \cdots \mathcal{O}_{\theta_N} \mathcal{U}\big(t_{\theta_N}, 0\big)|\rho^{SA}(0)\big\rangle\!\big\rangle. \tag{C3}$$

Here, P is the number of Fermi interchanges in the permutation of operators $\hat{O}_i$ by T_c, $\langle\langle I|$ is the Liouville space bra representation of the Hilbert space identity operator, θ_i are indices of operators $\hat{O}_i$ rearranged in such a way that $t_{\theta_1} > t_{\theta_2} > \cdots > t_{\theta_N}$ (t_{θ_i} is real time corresponding to contour variable τ_{θ_i}), $\mathcal{U}$ is the Liouville space evolution superoperator defined in Eq. (11), and $\mathcal{O}_{\theta_i}$ are the Liouville space superoperators corresponding to the Hilbert space operators $\hat{O}_i$,

$$\mathcal{O}_i|\rho\rangle\!\rangle = \begin{cases} \mathcal{O}_i^-|\rho\rangle\!\rangle \equiv \hat{O}_i\, \hat{\rho}, & \text{forward branch} \\ \mathcal{O}_i^+|\rho\rangle\!\rangle \equiv \hat{\rho}\, \hat{O}_i, & \text{backward branch.} \end{cases} \tag{C4}$$

Further details on evaluation of the multitime correlation functions can be found in Ref. [27].

Once single- and two-particle GFs of the reference system are known, the vertices required in Eq. (6) of the main text can be calculated from their definitions, given by Eq. (A12).

[1] Z. Ioffe, T. Shamai, A. Ophir, G. Noy, I. Yutsis, K. Kfir, O. Cheshnovsky, and Y. Selzer, Nat. Nanotechnol. **3**, 727 (2008).

[2] D. R. Ward, N. J. Halas, J. W. Ciszek, J. M. Tour, Y. Wu, P. Nordlander, and D. Natelson, Nano Lett. **8**, 919 (2008).

[3] D. R. Ward, D. A. Corley, J. M. Tour, and D. Natelson, Nat. Nanotechnol. **6**, 33 (2011).

[4] Z. Liu, S.-Y. Ding, Z.-B. Chen, X. Wang, J.-H. Tian, J. R. Anema, X.-S. Zhou, D.-Y. Wu, B.-W. Mao, X. Xu *et al.*, Nat. Commun. **2**, 305 (2011).

[5] N. Chiang, N. Jiang, D. V. Chulhai, E. A. Pozzi, M. C. Hersam, L. Jensen, T. Seideman, and R. P. V. Duyne, Nano Lett. **15**, 4114 (2015).

[6] J. Lee, N. Tallarida, X. Chen, P. Liu, L. Jensen, and V. A. Apkarian, ACS Nano **11**, 11466 (2017).

[7] N. L. Schneider, J. T. Lü, M. Brandbyge, and R. Berndt, Phys. Rev. Lett. **109**, 186601 (2012).

[8] E. Ćavar, M.-C. Blüm, M. Pivetta, F. Patthey, M. Chergui, and W.-D. Schneider, Phys. Rev. Lett. **95**, 196102 (2005).

[9] C. Chen, P. Chu, C. A. Bobisch, D. L. Mills, and W. Ho, Phys. Rev. Lett. **105**, 217402 (2010).

[10] Z. C. Dong, X. L. Zhang, H. Y. Gao, Y. Luo, C. Zhang, L. G. Chen, R. Zhang, X. Tao, Y. Zhang, J. L. Yang *et al.*, Nat. Photon. **4**, 50 (2010).

[11] H. Imada, K. Miwa, M. Imai-Imada, S. Kawahara, K. Kimura, and Y. Kim, Nature (London) **538**, 364 (2016).

[12] H. Imada, K. Miwa, M. Imai-Imada, S. Kawahara, K. Kimura, and Y. Kim, Phys. Rev. Lett. **119**, 013901 (2017).

[13] K. Kimura, K. Miwa, H. Imada, M. Imai-Imada, S. Kawahara, J. Takeya, M. Kawai, M. Galperin, and Y. Kim, Nature (London) **570**, 210 (2019).

[14] M. Galperin and A. Nitzan, Phys. Chem. Chem. Phys. **14**, 9421 (2012).

[15] M. Galperin, Chem. Soc. Rev. **46**, 4000 (2017).

[16] J. Gersten and A. Nitzan, J. Chem. Phys. **73**, 3023 (1980).

[17] R. Chikkaraddy, B. de Nijs, F. Benz, S. J. Barrow, O. A. Scherman, E. Rosta, A. Demetriadou, P. Fox, O. Hess, and J. J. Baumberg, Nature (London) **535**, 127 (2016).

[18] N. Kongsuwan, A. Demetriadou, R. Chikkaraddy, F. Benz, V. A. Turek, U. F. Keyser, J. J. Baumberg, and O. Hess, ACS Photon. **5**, 186 (2018).

[19] G. Cohen, E. Gull, D. R. Reichman, and A. J. Millis, Phys. Rev. Lett. **115**, 266802 (2015).

[20] A. E. Antipov, Q. Dong, J. Kleinhenz, G. Cohen, and E. Gull, Phys. Rev. B **95**, 085144 (2017).

[21] M. Ridley, V. N. Singh, E. Gull, and G. Cohen, Phys. Rev. B **97**, 115109 (2018).

[22] F. B. Anders, Phys. Rev. Lett. **101**, 066804 (2008).

[23] S. Schmitt and F. B. Anders, Phys. Rev. B **81**, 165106 (2010).

[24] U. Schollwöck, Rev. Mod. Phys. **77**, 259 (2005).

[25] U. Schollwöck, Ann. Phys. **326**, 96 (2011).

[26] C. Jung, A. Lieder, S. Brener, H. Hafermann, B. Baxevanis, A. Chudnovskiy, A. Rubtsov, M. Katsnelson, and A. Lichtenstein, Ann. Phys. **524**, 49 (2012).

[27] F. Chen, G. Cohen, and M. Galperin, Phys. Rev. Lett. **122**, 186803 (2019).

[28] A. N. Rubtsov, M. I. Katsnelson, and A. I. Lichtenstein, Phys. Rev. B **77**, 033101 (2008).

[29] H. Hafermann, C. Jung, S. Brener, M. I. Katsnelson, A. N. Rubtsov, and A. I. Lichtenstein, Europhys. Lett. **85**, 27007 (2009).

[30] A. E. Antipov, J. P. F. LeBlanc, and E. Gull, Phys. Proc. **68**, 43 (2015).

[31] G. Rohringer, H. Hafermann, A. Toschi, A. A. Katanin, A. E. Antipov, M. I. Katsnelson, A. I. Lichtenstein, A. N. Rubtsov, and K. Held, Rev. Mod. Phys. **90**, 025003 (2018).

[32] A. Rubtsov, M. Katsnelson, and A. Lichtenstein, Ann. Phys. **327**, 1320 (2012).

[33] E. G. C. P. van Loon, A. I. Lichtenstein, M. I. Katsnelson, O. Parcollet, and H. Hafermann, Phys. Rev. B **90**, 235135 (2014).

[34] E. G. C. P. van Loon, H. Hafermann, A. I. Lichtenstein, A. N. Rubtsov, and M. I. Katsnelson, Phys. Rev. Lett. **113**, 246407 (2014).

[35] E. G. C. P. van Loon, M. I. Katsnelson, and M. Lemeshko, Phys. Rev. B **92**, 081106(R) (2015).

[36] E. A. Stepanov, E. G. C. P. van Loon, A. A. Katanin, A. I. Lichtenstein, M. I. Katsnelson, and A. N. Rubtsov, Phys. Rev. B **93**, 045107 (2016).

[37] E. G. C. P. van Loon, F. Krien, H. Hafermann, E. A. Stepanov, A. I. Lichtenstein, and M. I. Katsnelson, Phys. Rev. B **93**, 155162 (2016).

[38] E. A. Stepanov, A. Huber, E. G. C. P. van Loon, A. I. Lichtenstein, and M. I. Katsnelson, Phys. Rev. B **94**, 205110 (2016).

[39] E. A. Stepanov, S. Brener, F. Krien, M. Harland, A. I. Lichtenstein, and M. I. Katsnelson, Phys. Rev. Lett. **121**, 037204 (2018).

[40] A. Kamenev, *Field Theory of Non-Equilibrium Systems* (Cambridge University Press, Cambridge, 2011).

[41] J. W. Negele and H. Orland, *Quantum Many-Particle Systems*, Vol. 68 (Addison-Wesley, Redwood City, CA, 1988).
[42] M. Wagner, Phys. Rev. B **44**, 6104 (1991).
[43] A. L. Fetter and J. D. Walecka, *Quantum Theory of Many-Particle Systems* (McGraw-Hill, New York, 1971).
[44] P. Coleman, *Introduction to Many-Body Physics* (Cambridge University Press, Cambridge, 2015).
[45] G. Stefanucci and R. van Leeuwen, *Nonequilibrium Many-Body Theory of Quantum Systems. A Modern Introduction.* (Cambridge University Press, Cambridge, 2013).
[46] D. Tamascelli, A. Smirne, S. F. Huelga, and M. B. Plenio, Phys. Rev. Lett. **120**, 030402 (2018).
[47] F. Mascherpa, A. Smirne, D. Tamascelli, P. F. Acebal, S. Donadi, S. F. Huelga, and M. B. Plenio, Phys. Rev. A **101**, 052108 (2020).
[48] E. Arrigoni, M. Knap, and W. von der Linden, Phys. Rev. Lett. **110**, 086403 (2013).
[49] A. Dorda, M. Ganahl, H. G. Evertz, W. von der Linden, and E. Arrigoni, Phys. Rev. B **92**, 125145 (2015).
[50] A. Dorda, M. Sorantin, W. v. d. Linden, and E. Arrigoni, New J. Phys. **19**, 063005 (2017).
[51] F. Chen, E. Arrigoni, and M. Galperin, New J. Phys. **21**, 123035 (2019).
[52] A.-P. Jauho, N. S. Wingreen, and Y. Meir, Phys. Rev. B **50**, 5528 (1994).
[53] L. Mühlbacher and E. Rabani, Phys. Rev. Lett. **100**, 176403 (2008).
[54] H.-P. Breuer and F. Petruccione, *The Theory of Open Quantum Systems* (Oxford University Press, Oxford, 2003).